Accepted Manuscript

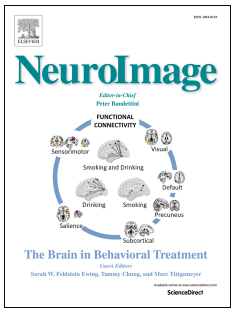

EEG microstates distinguish between cognitive components of fluid reasoning

Filippo Zappasodi, Mauro Gianni Perrucci, Aristide Saggino, Pierpaolo Croce, Pasqua Mercuri, Roberta Romanelli, Roberto Colom, Sjoerd J.H. Ebisch

PII: S1053-8119(19)30073-4

DOI: https://doi.org/10.1016/j.neuroimage.2019.01.067

Reference: YNIMG 15592

To appear in: *NeuroImage*

Received Date: 16 March 2018

Revised Date: 14 January 2019

Accepted Date: 26 January 2019

Please cite this article as: Zappasodi, F., Perrucci, M.G., Saggino, A., Croce, P., Mercuri, P., Romanelli, R., Colom, R., Ebisch, S.J.H., EEG microstates distinguish between cognitive components of fluid reasoning, *NeuroImage* (2019), doi: https://doi.org/10.1016/j.neuroimage.2019.01.067.

Title

EEG microstates distinguish between cognitive components of fluid reasoning
(NIMG-18-654 R2**)**

Authors

Filippo Zappasodi * [1,2], Mauro Gianni Perrucci * [1,2], Aristide Saggino [3], Pierpaolo Croce [1], Pasqua Mercuri [3], Roberta Romanelli [3], Roberto Colom [4], Sjoerd J.H. Ebisch ^ [1,2]

Affiliations

[1] Department of Neuroscience, Imaging and Clinical Sciences, G. d'Annunzio University of Chieti-Pescara, Chieti, Italy;
[2] Institute of Advanced Biomedical Technologies (ITAB), G. d'Annunzio University of Chieti-Pescara, Chieti, Italy;
[3] School of Medicine and Health Sciences, G. d'Annunzio University of Chieti-Pescara, Chieti, Italy;
[4] Universidad Autónoma de Madrid, Madrid, Spain.

* These authors equally contributed to the manuscript

^ Corresponding author: Sjoerd J.H. Ebisch; Department of Neuroscience, Imaging and Clinical Sciences; Institute of Advanced Biomedical Technologies (ITAB); G. d'Annunzio University of Chieti-Pescara; Via Luigi Polacchi 11; 66100 Chieti Scalo (CH); Italy; Tel. +39 0871 355 6949; Fax. +39 0871 355 6930; e-mail s.ebisch@unich.it

Abstract

Fluid reasoning is considered central to general intelligence. How its psychometric structure relates to brain function remains poorly understood. For instance, what is the dynamic composition of ability-specific processes underlying fluid reasoning? We investigated whether distinct fluid reasoning abilities could be differentiated by electroencephalography (EEG) microstate profiles. EEG microstates specifically capture rapidly altering activity of distributed cortical networks with a high temporal resolution as scalp potential topographies that dynamically vary over time in an organized manner. EEG was recorded simultaneously with functional magnetic resonance imaging (fMRI) in twenty healthy adult participants during cognitively distinct fluid reasoning tasks: induction, spatial relationships and visualization. Microstate parameters successfully discriminated between fluid reasoning and visuomotor control tasks as well as between the fluid reasoning tasks. Mainly, microstate B coverage was significantly higher during spatial relationships and visualization, compared to induction, while microstate C coverage was significantly decreased during spatial relationships and visualization, compared to induction. Additionally, microstate D coverage was highest during spatial relationships and microstate A coverage was most strongly reduced during the same condition. Consistently, multivariate analysis with a leave-one-out cross-validation procedure accurately classified the fluid reasoning tasks based on the coverage parameter. These EEG data and their correlation with fMRI data suggest that especially the tasks most strongly relying on visuospatial processing modulated visual and default mode network activity. We propose that EEG microstates can provide valuable information about neural activity patterns with a dynamic and complex temporal structure during fluid reasoning, suggesting cognitive ability-specific interplays between multiple brain networks.

Key words

EEG, microstates, fluid reasoning, cognitive abilities, visuospatial

1. Introduction

The understanding of intelligence and brain function underlying its cognitive processes is of particular interest in psychology and neuroscience. General intelligence (g) is a key psychometric construct that quantifies the positive correlation among widely diverse cognitive tasks. Fluid reasoning is considered a central cognitive ability for g and is represented by the fluid intelligence factor Gf (Carroll, 1993; Cattell, 1963; Deary et al., 2010; Jensen, 1980; Jensen, 1998; Spearman, 1927). Fluid reasoning refers to logical and abstract thinking, understanding relationships between stimuli, and solving problems in novel situations (Cattell, 1987). Emphasizing its socio-economic relevance, individual performance on fluid reasoning tasks predict a large variety of cognitive, developmental, aging, educational and health effects (Alexander et al., 1997; Batty et al., 2007; Calvin et al., 2017; Calvin et al., 2011; Deary et al., 2005; Gottfredson, 1997; Gray & Thompson, 2004; Hunt, 2011; Matsuda & Saito, 1998; Whalley et al., 2004; Buckley et al., 2018).

A vast amount of neuroimaging studies focused on intelligence, and several also specifically on fluid reasoning, to explain general cognitive performance (Barbey et al., 2012; Basten, 2015; Colom, Jung, & Haier, 2006; Deary et al., 2010; Duncan, 2010; Duncan et al., 1995; Duncan et al., 2000; Glascher et al., 2010; Gray et al., 2003; Jung & Haier, 2007; Lee et al., 2006; Perfetti et al., 2009; Prabhakaran et al., 1997; Roca et al., 2010; Santarnecchi et al., 2015; Song et al., 2008; Woolgar et al., 2010). However, it remains unclear how the psychometric structure of intelligence relates to brain function, especially how cognitive tasks draw on a combination of both common and unique abilities (Colom, Burgaleta, et al., 2013; Colom & Quiroga, 2009; Glascher et al., 2009; Roman et al., 2014). This is relevant, since psychometric evidence suggests that, although g can account for a large proportion (50% or more) of the variance in individual cognitive abilities, specific cognitive abilities show a considerable amount (20 to 50%) of unique variance (Deary et al., 2010). Moreover, the effect of using different tasks to measure fluid reasoning, each requiring particular cognitive abilities, remains poorly understood (Burgess et al., 2011; Gazzaley et al., 2005). Studies still need to characterize the dynamic composition of ability-specific and common processes to understand the neuro-functional mechanisms of fluid reasoning.

The influential, empirically-based psychometric framework proposed by Carroll (1993) provides useful insight into the relationship between task-common and task-specific cognitive functions by showing that cognitive abilities are organized according to a stratified structure. A discrete number of specific cognitive abilities ("narrow" factors) located on the lowest stratum have high loadings on Gf on the second stratum, but also some uniqueness. Gf in turn loads on the general factor g located on the first stratum.

fMRI findings started to clarify this framework by showing that specific cognitive abilities with high loadings on Gf recruit partially unique brain circuits (Ebisch et al., 2012) and that task-common regions interact in a context-dependent way with task-specific brain regions during distinct Gf tasks (Ebisch et al., 2013). This is consistent with neuroimaging findings suggesting that abstract reasoning abilities essentially rely on an integrative functioning of multiple task-common and task-specific brain networks including lower levels of perceptual processing (Barbey et al., 2014; Burgaleta et al., 2014; Cole et al., 2015; Colom et al., 2006; Deary et al., 2010; Duncan, 2010; Gray et al., 2003; Roca et al., 2010; Roman et al., 2014; Santarnecchi & Pascual-Leone, 2017; Woolgar et al., 2010; Brumback et al., 2004; Buschman et al., 2011; Melnick et al., 2013; Narr et al., 2007; Soulieres et al., 2009).

Although functional magnetic resonance imaging (fMRI) is efficient in capturing neural activity with high spatial precision, its low temporal resolution is a drawback. Fluid reasoning abilities as usually assessed by common psychometric tests are relatively complex (e.g., Raven Progressive

Matrices). Different cognitive processes could be recruited during early and late processing stages of fluid reasoning tasks, while the temporal structure of such processes is not always known (Hayes, 2015).

The dynamic variation of electrical neuronal activity likely contains relevant complementary information. Electroencephalography (EEG) is suitable to capture the macroscopic temporal dynamics of brain electrical activity with a very high temporal resolution (~1 ms), allowing to track the cerebral dynamics with the temporal detail of the neuronal processes. Post-synaptic excitatory and inhibitory potentials are the main sources of the EEG signals (Lopes da Silva & van Rotterdam, 2012). EEG oscillations reflect rhythmic fluctuations of these excitation and inhibition potentials in neuronal ensembles (Lopes da Silva, 1991).

By multichannel EEG, it is possible to detect periods in which the electric potential topographic configuration on the scalp is stable (Britz et al., 2010; Michel & Koenig, 2017). This phenomenon allows to describe neuronal activity by a limited number of rapidly transitioning scalp potential topographies, or "maps", that remain stable for a brief period of time (60-120 ms) (Michel & Koenig, 2017). Such epochs of topographic stability have been referred to as "microstates" (Lehmann, 1987; Lehmann & Koenig, 1997; Pascual-Marqui et al., 1995). In other words, microstates capture altering activity of distributed cortical networks as global patterns of scalp potential topographies that dynamically vary over time in an organized manner (Lehmann & Koenig, 1997; Lehmann & Michel, 2011).

Initial studies converged on the existence of four microstates across subjects (Britz et al., 2010; Brodbeck et al., 2012; Koenig et al., 1999), although it also has been recommended to determine the appropriate number for each dataset based on the explained variance. The four microstates exhibited highly similar topographies across studies and were labelled as class A, B, C, and D (Koenig et al., 1999; Michel & Koenig, 2017). Microstate map A exhibits a left-right orientation, map B exhibits a right-left orientation, map C exhibits an anterior-posterior orientation, and map D exhibits a fronto-central maximum. Although several studies identified more maps, these four maps seem to consistently dominate the data across different age ranges, conditions, and pathological states (Khanna et al., 2015; Koenig et al., 1999).

No complete consensus exists on the cerebral sources of the four microstates, yet. One study found a high degree of overlap for the four microstates, particularly in the anterior and posterior cingulate cortices and the left and right occipital/parietal areas (Pascual-Marqui et al., 2014). Another study showed that common areas of the four microstates corresponded to main structural and functional brain hubs, including anterior and posterior cingulate cortices, precuneus, superior frontal cortex, supramarginal gyrus, dorsal superior prefrontal cortex, and insula (Custo et al., 2017).

Integration of EEG with fMRI data provided further insight into the sources of the microstates. Some data suggest that microstate A reflects auditory network activity, microstate B visual network activity, microstate C control network activity and microstate D dorsal attention network activity (Britz et al., 2010). However, other results suggest that microstate C rather reflects activity in the default mode network (Michel & Koenig, 2017; Seitzman et al., 2017) and microstate D is associated with reflexive aspects of attention, focus switching, and reorientation, processes occurring more frequently during rest than during single-goal-directed tasks (Milz et al., 2016).

Only very little evidence is available regarding the relation between microstates and fluid reasoning. A recent study (Santarnecchi et al., 2017) showed that scores on certain fluid reasoning tests (Raven Advances Progressive Matrices, RAPM, Raven, 2003; Sandia logical matrices, Matzen et al., 2010) inversely co-varied with microstate C, whereas fluid reasoning scores based on other

fluid reasoning tests (BOMAT, Hossiep et al., 1999; Sandia relational matrices, Matzen et al., 2010) was associated with microstate B. The latter possibly reflects the involvement of abilities related to visual search, feature selection and visuospatial attention. Given that Santarnecchi and colleagues (2017) measured microstates during a resting state without a particular cognitive task, and only few studies addressed microstate modulation during task performance (Milz et al., 2016; Seitzman et al., 2017) or otherwise related to task performance (Muthukrishnan et al., 2016), it remains an open issue how microstates are involved in actual fluid reasoning. Moreover, a relevant question is whether EEG microstates distinguish between psychometric subcomponents of fluid reasoning.

The present study aims at investigating whether and how distinct fluid reasoning subcomponents ("narrow" factors) could be typified by task-specific microstate profiles. For this purpose, EEG recordings were performed simultaneously with fMRI scanning (see Ebisch et al., 2013; Ebisch et al., 2012) during fluid reasoning tasks: induction, visualization and spatial relationships (Carroll, 1993). The fluid reasoning tasks were psychometrically validated warranting that they significantly loaded on Gf and were characterized by unidimensionality, though represented psychometrically distinguishable cognitive factors. The fluid reasoning tasks were accurately matched regarding difficulty and stimuli characteristics. EEG analyses comprised the comparison of the coverage, duration and occurrence parameters of the different microstates between the fluid reasoning tasks as well as the application of a multivariate approach to classify the distinct tasks based on the microstate parameters.

We hypothesized an increase of microstate B properties during the conditions Visualization and Spatial Relationships, given the stronger emphasis on visuospatial processing in these tasks, compared to the Induction task. Microstate C involvement was expected to be decreased during all the fluid reasoning conditions, compared to a visuomotor control task, reflecting a general suppression of the default mode network during cognitively demanding tasks. Finally, microstate D metrics could be enhanced by all the fluid reasoning conditions, compared to the visuomotor control condition, associated with stronger demands on visuospatial orienting with respect to the visual fluid reasoning stimuli, but it could be especially recruited during the Spatial Relationships task due to increased demands on visuospatial processing. Differential microstate profiles for the distinct tasks were further expected to be confirmed by above chance classification of the tasks using a multivariate approach. Regarding the relationship with fMRI data, we hypothesized that involvement of microstate B positively correlated with neural activity in visual cortices, microstate C negatively correlated with common activity in default mode network, and microstate D positively correlated with common activity in the dorsal attention network.

2. Material and methods

2.1 Participants

Twenty university students (age range: 20–24), all healthy, female and right-handed (Edinburgh Handedness Inventory score > 0.85), participated in the present EEG-fMRI study according to the procedures described in Ebisch et al. (2012) as the studies concern the same participants. Two participants from the original study (N = 22; Ebisch et al., 2012) were excluded, because of technical problems with the EEG data acquisition. All participants provided their written informed consent after full explanation of the study's procedure, in line with the Declaration of Helsinki. The experimental protocol was approved by the local institutional ethics committee.

2.2 Calibration study of the fluid reasoning test

The fluid reasoning tasks administered during EEG-fMRI acquisition were extracted from the initial item bank produced for the construction of the Fluid Intelligence Test (FIT) created by R.R. and A.S. (Romanelli & Saggino, 2014). The FIT items used for the present study consisted of a bank of 220 items, randomly assigned to two parallel forms (FIT1 and FIT2). According to Carroll's framework (Carroll, 1993), four subtests were included in the FIT: Induction (IN), Visualization (VZ), Spatial Relationships (SR) and Quantitative Reasoning. IN is defined by the ability to inspect a class of stimuli and then to infer/induce/deduce a common characteristic underlying these materials; VZ involves manipulating or transforming the image of spatial patterns into other visual arrangements; SR is based on the ability to perceive spatial patterns or to maintain orientation with respect to objects in space. Because of the very different nature of the stimuli, the Quantitative Reasoning factor (the ability to reason deductively or inductively based on mathematical properties and relations) was not included in the EEG-fMRI study.

The FIT was validated by a calibration study showing a proper internal consistency and a good construct validity. FIT items had a mean difficulty level, good discrimination and an acceptable level of guessing. Unidimensionality and local independence assumptions were met for both forms. Local independence implicates that all items are correlated with one another, because they measure the same latent trait. If we keep the latent trait constant, all items will be independent as their relationship is only determined by that specific latent trait. Internal consistency reliabilities for the FIT total scores were high: FIT-1 had a KR-20 coefficient of 0.95, while FIT-2 a KR-20 coefficient of 0.94. Regarding the subtests, KR-20 coefficients of the FIT-1 were 0.89 for IN, 0.85 for VZ and 0.82 for SR. KR-20 coefficients of the FIT-2 were 0.78 for IN, 0.82 for VZ and 0.81 for SR. A more detailed description of the calibration study and its results is provided in the supplementary material and in Ebisch et al. (2012).

The two parallel forms of the FIT (total scores) correlated significantly with RAPM total score ($r_{FIT-1;APM} = 0.55$; $r_{FIT-2;APM} = 0.72$) in a subgroup of 300 participants. The lower correlation between FIT-1 and RAPM could be attributed to a low correlation of the quantitative reasoning subtest (included in the FIT, but not in the present study) with RAPM (r = 0.23). Indeed, the individual FIT subtests included in the present EEG-fMRI study correlated significantly and consistently with RAPM scores ($r_{IN-1;APM} = 0.50$; $r_{IN-2;APM} = 0.60$; $r_{VZ-1;APM} = 0.50$; $r_{VZ-2;APM} = 0.58$; $R_{RS-1;APM} = 0.53$; $r_{RS-2;APM} = 0.57$), thus, further showing that all the subtests are relevant for fluid reasoning and Gf. The subtests were also highly inter-correlated. Within FIT-1, the following correlations could be observed: $r_{in-vz} = 0.67$, $r_{in-sr} = 0.70$, and $r_{vz-sr} = 0.61$. Within FIT-2, the following correlations could be observed: $r_{in-vz} = 0.61$, $r_{in-sr} = 0.66$, and $r_{vz-sr} = 0.60$.

2.3 Stimuli

Seventy-five visual items were extracted from the FIT item bank for the fMRI-EEG study; 25 items from each subtest reflected a specific first-order Gf factor: Induction, Visualization, and Spatial Relationships. These factors were characterized by identical visual characteristics and type of task. The experimental conditions constituted by items selected across the different factors were matched for difficulty according to Item Response Theory (IRT) (Bock, 1997; Embreston, 2000) parameters obtained by the calibration study (see Table 1). In the present EEG-fMRI study, IN included 10 items from FIT-1 and 15 items from FIT-2, VZ included 14 items from FIT-1 and 11 from FIT-2, and SR included 13 items from FIT-1 and 12 items from FIT-2. A Chi-Square test showed that items from FIT-1 and FIT-2 were equally distributed over the conditions; $p = 0.50$).

All test items of IN, VZ and SR consisted of black and white line drawings. Every item in the test has four response alternatives indicated by a letter (a, b, c and d), among which participants have to choose the correct answer. The problem of each Gf item consists in finding the response alternative

that represents the most suitable answer to the problem. Questions preceding each problem were visually presented on the screen like, for example, “Which figure completes the series?” or “Which is the missing figure?”.

For the fMRI-EEG experiment, 25 visual Control items (CC) were added to control for the visual aspects, oculomotor activity and motor response, without including a reasoning ingredient. The control items consisted of modified line drawings based on those in the IN, VZ and SR conditions. At an unpredictable moment (average: 14 s; range: 7–28 s), a letter (A, B, C and D) appeared in a random place in the drawing. The instruction preceding each control item was “Study the figure and indicate, by means of a button press, which letter appears in the drawing”.

2.4 Procedure

A computerized fluid reasoning test was developed including the items as described above. Item order during the experiment was randomized. Each test item was preceded by a question mark (1000 ms) and a specific question/instruction (2000 ms). Trial duration was self-paced, depending on the time required by the participant to find the correct answer (maximum = 40 s). Participants had two buttons in their left hand (middle and index finger) and two buttons in their right hand (index and middle finger) representing from left to right the letters a–d. Participants were asked to press a button to indicate the correct answer to each test item. After the button press, the test item disappeared from the screen to proceed with the intertrial interval. In case the participant failed to press a button within 40 s, the item disappeared automatically to proceed with the intertrial interval.

The intertrial interval consisted of a grey screen and a fixation cross that gradually appeared in the center of the screen over a period of 5000 ms. The onset of the fixation cross varied between 1000 and 5000 ms and the cross got either brighter or darker, compared to the background colour. Participants were required to indicate whether the cross became darker or brighter by means of a button press with their left or right index finger, respectively. This basic task was added to the intertrial interval for interrupting the reasoning processes related to the preceding test items, because a pilot study revealed that participants tend to continue reasoning about the preceding test item during the intertrial interval. The next test item followed the intertrial interval automatically after a fixed period of 15 s. The entire experiment consisted of 6 separated fMRI-EEG runs, with 2 runs for each fluid reasoning condition and 12 or 13 fluid reasoning items/run. Control items were randomly inserted in these runs. The total (effective) duration of the fMRI experiment was 55 min on average with a minimum of 45.5 min and a maximum of 67.5 min. Prior to the fMRI session, a practice session was performed outside the scanner to train the participants on the task. The time line of the experimental procedure and the visual stimuli are visualized in Ebisch et al. (2012).

2.5 EEG-fMRI data acquisition

During a single session measurement, EEG was recorded simultaneously with fMRI at 3T using MR compatible devices.

EEG data were recorded by Brain Vision Recorder (Brain Products, GmhB, Germany) using a 64-channel MR compatible EEG system with an MR compatible amplifier and a synchronisation box (Brain Products, GmhB, Germany). The EEG cap (BrainCap MR, EasyCap GmbH, Germany) consisted of 62 scalp electrodes, ring-type sintered nonmagnetic Ag/AgCl electrodes, distributed according to the 10–10 system and two additional channels dedicated for recording the electrocardiogram and the electro-oculogram. The reference electrode was predefined in the cap and positioned in correspondence of the FCz electrode. The ground electrode was predefined and placed at Iz. Impedances at all recording electrodes were kept below 10 kΩ by means of an electrode paste.

The resolution and dynamic range of the EEG acquisition system were 100 nV and ± 3.2 mV, respectively. Data were sampled at 5000 Hz, with a band-pass filter of 0.016-250 Hz. The Sync Box device (Brain Products, GmhB, Germany) was used to synchronize the hardware clock of the EEG with the MRI scanner's gradient switching system.

Functional MRI data were recorded using a 3 T Philips Achieva scanner at the Institute of Advanced Biomedical Technologies (ITAB), Chieti, Italy. An initial T1-weighted anatomical (3D MPRAGE pulse sequence; 1 mm isotropic voxels) and T2*-weighted functional data were collected with an eight channel phased array head coil. EPI data (gradient echo pulse sequence) were acquired from 31 slices (3.5×2.875×2.875 mm^3 resolution, TR=1950 ms, TE=62 ms, SENSE factor=2, flip angle=80°, field of view=230 mm). Slices were oriented parallel to the AC–PC axis of the observer's brain.

2.6 EEG data pre-processing

The EEG data were pre-processed using Brain Vision Analyzer (Brain Products, Munich, Germany). Gradient artefact correction was performed by means of the method proposed by Allen et al. (2000) and incorporated integrated in Brain Vision Analyzer v.2.0. Data were down-sampled to 500 Hz and exported in matlab format and processed by using a self-developed software implemented in MATLAB (Mathworks, Sherborn, MA). They were digitally filtered in the band 0.5–50 Hz using a Chebyshev II-type filter with 40 dB attenuation and zero-phase distortion. After visually checking them for the elimination of movement artefacts and noisy channels from the whole data set, by setting a threshold of 100 microvolt for all subjects, a procedure based on Independent Component Analysis (Comon, 1994; Hyvärinen, 2001; James, 2004) was used for the rejection of the ballistocardiographic artefact, ocular movement and the residual imaging artefact from the filtered EEG recordings (Mantini et al., 2007; Vanderperren et al., 2010).

2.7 EEG Microstates data analysis

Only trials with a successful response were utilized for the microstate analysis. We used a modified version of the k-means clustering algorithm (Pascual-Marqui et al., 1995). A Butterworth filter of 2nd order was firstly used to forward and back filter the 62 EEG signals between 1 and 30 Hz and data were down-sampled to a sampling rate of 125 Hz. For each subject and for each condition (CC, IN, SR, VZ), the inter-trial intervals were removed and the remaining concatenated data were divided in epochs of 2 second duration. The Global Field Power (GFP) was calculated for each time frame in the resulting concatenated EEG time series (Figure 1). Specifically, the GFP is the standard deviation of the EEG signal across electrodes and represents a global measure of the EEG strength. For each 2-second window, only the EEG data corresponding to the maxima of GFP were then submitted to a clustering algorithm. Indeed, these peaks correspond to periods of highest topographic stability, when the probability to observe a transition is more likely (Murray, Brunet, & Michel, 2008). For each subject and for each condition, the k-means algorithm was repeated varying the number of clusters (k) from 1 to 12. The optimal number of k was chosen by estimating, for each repetition, the Krzanowski-Lai (KL) criterion and by choosing the number of clusters corresponding to the second KL maximum value (Murray et al., 2008). With this criterion, the optimal number of microstates was found to be equal to 4.

From the above procedure, four maps for each subject and for each condition were obtained (Figure 1). To individuate a correspondence of individual microstates topographies across subjects and to calculate the mean microstate maps for each condition, the following iterative procedure was applied (Koenig et al., 1999). Separately for each condition (CC, IN, SR, VZ), a number of 4 initial maps were randomly chosen as template set. The maps of each subject were spatially correlated

with the template maps and assigned to one map of the template on the basis of the best spatial correlation values. A new template set was then obtained by averaging all the maps assigned to the same template. With the new template, the procedure of spatial correlation and map assignment was repeated, and a new template set obtained. The iteration spatial correlation/assignment/average and new template was repeated until the best fit was found and the new assignment did not change anymore. The maps resulting from this procedure (four maps for each condition) were paired between the 4 conditions (CC, IN, SR, VZ) by ensuring the minimal maps dissimilarity and were labelled as A, B, C, D in accordance to the topographies previously found in literature (see Koenig et al., 1999, for a complete description). In this way, a total of sixteen maps (four maps, labelled A, B, C, and D for each of the four conditions CC, IN, SR, VZ) were obtained. The four global maps representing all the four conditions were computed by averaging the corresponding maps across conditions.

To compute microstates metrics, the obtained global maps were fitted backward to the original data calculating the spatial correlation between each template and the topography at each time instant corresponding to the maximum value of GFP. Such a procedure allows to represent the EEG time course in terms of sequence of microstates and to extrapolate variables of interest.

For each subject, for each microstate class and for each condition, the following metrics were calculated (Brunet et al., 2011; Lehmann, 1987):

1) mean microstate duration (ms): the average duration or lifespan of each microstate calculated as the average length of time that a given microstate remains stable whenever it appears (Lehmann & Koenig, 1997). As such, the microstate duration index can be interpreted as reflecting the stability of its underlying neural assemblies.

2) mean microstate occurrence (N): the frequency of occurrence of each microstate calculated as the average number of times per second that the microstate becomes dominant during the recording period (Lehmann & Koenig, 1997). Microstate occurrence could reflect the tendency of its underlying neural generators to become activated.

3) mean microstate coverage (%): the coverage of a microstate calculated as the fraction of total recording time (covered analysis time) that the microstate is dominant (Lehmann, 1987).

Mean Global Explained Variance (GEV) was also obtained for all the microstate classes, as the sum of the explained variances weighted by the global field power at each moment in time. The metrics were separately computed for each condition (CC, IN, SR, VZ). Both microstate coverage and GEV reflect the relative time coverage of its underlying neural generators compared to others.

2.8 Microstate Statistical Analysis

Prior to statistical analysis, delta scores were calculated for each microstate metric (coverage, duration and occurrence) in the experimental conditions by subtracting microstate scores of the control condition, CC, from the scores of the IN, RS and VZ tasks.

Firstly, to test whether microstate parameters (coverage, duration and occurrence) during the fluid reasoning tasks were significantly different from the control condition, one-sample t-tests were performed on the delta scores ($p < 0.05$ after Bonferroni correction).

Secondly, to assess differences across different experimental conditions, repeated measure analyses of variance (ANOVAs) were separately performed for each microstate metric delta score. A 4 X 3 design was applied, with Microstate Class (A, B, C, D) and Conditions (IN, SR, VZ) as within-subject factors. Greenhouse-Geisser correction has been applied if the sphericity assumption was not valid. When an interaction Microstate Class * Conditions was found, reduced models were

separately applied for each microstate class, with fluid reasoning conditions as within-subject factor. Post-hoc paired samples t-tests were carried out to assess significant differences of delta microstate class metric among conditions. Post-hoc comparisons were Bonferroni corrected.

2.9 Multivariate Analysis

In addition to canonical microstates analysis, a multivariate approach was separately applied to each metric (duration, occurrence, coverage) to classify the conditions IN, RS and VZ. A support vector machine (SVM) classifier at single trial level was used with a leave-one-out cross-validation scheme (Cawley and Talbot, 2004). SVM is a supervised learning algorithm that can be employed for binary linear classification. Since in our case three different conditions need to be classified, a one versus all approach was performed (Rifkin and Klautau, 2004). In general, a SVM model is a representation of points in the features space (in our case, microstates metrics for each trial and for each subject) mapped so that different classes are divided by a gap that is as wide as possible (Cortes and Vapnik, 1995).

At each cross-validation step, the classifier was trained with all the single trials of 19 subjects and tested with all the single trials of the excluded subject. SVM analysis was computed in MatLab with the following setting: Auto-scale, 1; Box-constraint, 1; Kernel function, Linear; Method Sequential Minimum Optimization. The total number of trials for classification analysis was 650 for IN, 724 for RS and 564 for VZ. As an indicator of the classification performance, the global accuracy (ratio between true positive and number of total tested samples) was calculated and to obtain a confusion matrix. This matrix shows on the rows the number of predicted classes and on the columns the number of true cases.

2.10 fMRI Statistical Analysis

A boxcar waveform representing the stimuli (predictors: question mark, question, test items according to the experimental conditions with a successful response, test items with an unsuccessful response, button press; see also Ebisch et al., 2012) was convolved with the default Boynton hemodynamic response function to account for the hemodynamic delay. The intertrial interval was not modelled and was used as a baseline. Prior to statistical analysis calculation, a percent signal change normalization of the fMRI time series was performed. This scaling normalizes a voxel time course by transforming the mean signal to a value of 100 and letting fluctuate the individual values around that mean as percent signal deviations. Normalized fMRI responses allow to indicate differences across conditions regardless of the variability in the fMRI signal across subjects, scanning sessions, and voxels. The parameters (beta-values) estimated in individual-subject GLM analyses were entered in a second-level voxel-wise random effect group analysis in order to search for voxel clusters showing consistent effects (differences in BOLD response between the experimental conditions) for the whole group of participants. To account for spatial variability among participants, spatial smoothing with a Gaussian kernel of 6 mm full width half-maximum was applied to the functional images. To identify voxel clusters in which brain activity significantly ($p < 0.01$ corrected) correlated with microstate parameters, whole-brain voxel-wise covariance analyses were performed.

Each fluid reasoning condition was contrasted separately with the control condition, while using microstate parameters (average differential value: fluid reasoning task minus control condition) as a covariate. The focus was specifically on microstate coverage, given that this parameter specifically distinguished between the fluid reasoning tasks (see results, paragraphs 3.3 – 3.6). The p-value of the statistical maps ($p < 0.001$) and an estimate of the spatial correlation of voxels were used as input in a Monte Carlo simulation to access the overall significance level and to determine a cluster

size threshold in order to obtain the significance level of $p < 0.01$ corrected for multiple comparisons (Cox et al., 1996; Forman et al., 1995). This procedure computes a cluster-size threshold taking into account the probability of detecting false positive (noise-only) clusters for a given voxel-wise p-value threshold by simulating noise-only random volumes (1000 simulations), thresholding and clustering them, and counting statistics of how often data survives these processes at various threshold combinations (per-voxel and cluster-size).

3. Results

3.1 Behavioral analysis

Differences between the fluid reasoning conditions with respect to reaction times (of correct responses) and errors (percentage trials with incorrect responses) were tested by means of ANOVAs with condition (IN, SR, VZ) as within-subject factor. No significant main effect was detected for reaction times ($F_{2,38}$= 1.643, p= 0.21), implying that the conditions were comparable for reaction time. A significant main effect was found for errors ($F_{2,38}$= 3.432, p= 0.04), but post-hoc paired sample t-tests failed to detect significant differences between the conditions (all p> 0.07 after Bonferroni correction).

3.2 EEG results: microstate identification

According to the KL criterion, the optimal number of templates was found to be equal to 4 for each condition (CC, IN, SR, VZ). The global explained variance by the four microstates was 75 ± 2.2 % for the control condition, 74 ± 2 % for the Induction condition, 76 ± 1.8 % for the Spatial Relationships condition and 75 ± 1.7% for the Visualization condition. Explained variance was not different across conditions ($p > 0.200$). The four topographic maps of the microstates (labelled as A, B, C and D, according to literature) are visualized in Figure 2a.

3.3 EEG results: microstate coverage during the fluid reasoning conditions

One-sample t-tests on the delta coverage scores (see red dots in Figure 2b) showed that, compared to CC: microstate A was significantly decreased during SR ($p < 0.02$ after Bonferroni correction); microstate B was significantly increased during SR and VZ ($p < 0.005$ after Bonferroni correction); microstate C was significantly decreased during SR ($p < 0.005$ after Bonferroni correction); microstate D was significantly increased during SR ($p < 0.005$ after Bonferroni correction).

Repeated measures ANOVA with the microstate delta coverage scores of the fluid reasoning conditions (factor with three levels: IN, SR and VZ) and the microstates (factor with four levels: A, B, C, D) as within-subject variables showed a significant main effect of microstate ($F_{3,114}$ = 321.999; p = 0.019) as well as a significant microstate * condition interaction effect ($F_{6,114}$ = 48.814; p = 0.007), but no significant main effect of condition ($F_{2,114}$ = 63.439; p = 0.070). No significant covariance effect was detected for errors (p> 0.4) or for reaction times (p> 0.1).

Reduced models applied on the separate microstates based on repeated measures ANOVA with the microstate delta scores of the 3 conditions (IN, SR and VZ) as within-subject variables yielded significant main effects for microstate A ($F_{2,38}$ = 6.466, p = 0.005), microstate B ($F_{2,38}$ = 11.463, p = 0.001), microstate C ($F_{2,38}$ = 16.106, p = 0.001), and microstate D ($F_{2,38}$ = 21.107, p = 0.001). Thus, coverage of all microstates differentiated between the fluid reasoning conditions.

To further test for specific differences in microstate delta scores between the Gf conditions, post-hoc paired-sample t-tests were performed (Figure 2b). Concerning microstate A, a significant difference was found between SR and VZ ($p < 0.02$ after Bonferroni correction), but not between VZ and IN or between SR and VZ ($p > 0.5$ and $p > 0.06$, respectively). This suggested a stronger reduction of microstate A coverage during the SR condition.

Microstate B was significantly higher during both SR and VZ, compared to IN ($p < 0.005$ after Bonferroni correction), whereas no difference was found between SR and VZ ($p > 0.5$), indicating a higher coverage of microstate B during the SR and VZ conditions.

Microstate C coverage delta score was significantly lower during SR and VZ, compared to IN ($p <$ 001 and $p < 0.03$ after Bonferroni correction, respectively), but not different between SR and VZ ($p > 0.07$). This implied stronger reduction in microstate C coverage during SR and VZ.

Finally, SR showed a stronger coverage delta score for microstate D than both VZ ($p < 0.001$ after Bonferroni correction) and IN ($p < 0.001$ after Bonferroni correction), whereas IN and VZ did not differ ($p > 0.4$). Microstate D coverage was specifically increased during the SR condition.

Mean delta coverage scores and 95% confidence intervals (CIs) for the different microstates and conditions are provided in Supplementary Table 3.

3.4 EEG results: microstates duration during the fluid reasoning conditions

One sample t-tests on the delta duration scores (see Figure 2c) showed that duration of all microstates (A, B, C, D) was reduced during all the fluid reasoning conditions (IN, SR, VZ), compared to CC (all $p < 0.001$ after Bonferroni correction; see red dots in Figure 2c).

Repeated measures ANOVA with the microstate duration delta scores of the fluid reasoning conditions (factor with three levels: IN, SR and VZ) and the microstates (factor with four levels: A, B, C, D) as within-subject variables showed a significant main effect of microstate ($F_{3,114} = 321.999$; $p = 0.019$) as well as a significant microstate * condition interaction effect ($F_{6,114} = 48.814$; $p = 0.007$), but no significant main effect of condition ($F_{2,114} = 63.439$; $p = 0.07$). No significant covariance effect was detected for errors ($p > 0.4$) or for reaction times ($p > 0.1$).

Reduced models applied on the separate microstates based on repeated measures ANOVA yielded a significant main effect of fluid intelligence condition for microstate A ($F_{2,38} = 6.899$, $p = 0.004$), microstate B ($F_{2,38} = 3.433$, $p = 0.048$), microstate C ($F_{2,38} = 6.752$, $p = 0.006$), but not for microstate D ($F_{2,38} = 0.798$, $p = 0.4$). This suggested that duration of microstates A, B and C differentiated between the fluid intelligence conditions.

To further test for specific differences in microstate delta scores between the Gf conditions, post-hoc paired-sample t-tests were performed. Concerning microstate A, a significant difference was found between SR and VZ ($p < 0.05$ after Bonferroni correction), but not between VZ and IN or between SR and VZ ($p > 0.3$ and $p > 0.01$, respectively). This suggested a stronger reduction of microstate A duration during the SR condition.

Microstate B was significantly lower during IN, compared to VZ ($p < 0.05$ after Bonferroni correction), whereas no difference was found between SR and VZ or between IN and SR (both $p >$ 0.5), indicating a stronger reduction of microstate B during the IN condition.

Finally, microstate C was significantly lower during SR, compared to IN ($p < 001$ after Bonferroni correction), but not different between SR and VZ or between VZ and IN ($p > 0.01$ and $p > 0.5$, respectively). This implied a stronger reduction in microstate C duration during SR.

Mean delta duration scores and 95% CIs for the different microstates and conditions are provided in Supplementary Table 4.

3.5 EEG results: microstates occurrence during the Gf conditions

One sample t-tests on the delta occurrence scores showed that occurrence of all microstates (A, B, C, D) was not different during the fluid intelligence conditions (IN, SR, VZ), compared to CC (all $p > 0.2$) in all cases, except for microstate B during IN ($p < 0.005$ after Bonferroni correction). The latter indicated a reduction in microstate B during IN, compared to CC.

Repeated measures ANOVA with the microstate occurrence delta scores of the Gf conditions (factor with three levels: IN, SR and VZ) and the microstates (factor with four levels: A, B, C, D) as within-subject variables showed a significant main effect of microstate ($F_{3,114} = 9.424$; $p < 0.001$), but neither a significant effect of condition ($F_{2,114} = 1.860$; $p = 0.18$) nor a significant microstate * condition interaction effect ($F_{6,114} = 1.437$; $p = 0.229$).

Mean delta occurrence scores and 95% CIs for the different microstates and conditions are provided in Supplementary Table 5.

3.6 EEG results: multivariate classification analysis

The coverage metric resulted in a good overall classification accuracy of 72.45 % in distinguishing fluid reasoning conditions (IN, SR, VZ). The confusion matrix, reported in Figure 3, shows the classification performances for each fluid reasoning condition with a specific accuracy of 69.2% for IN, 71.8% for RS, and 77.0% for VZ. By contrast, global accuracy of the classification was below 35% for the duration and occurrence metrics.

3.7 Correlations between microstates and fMRI data

Given that microstate coverage most clearly distinguished between the fluid reasoning tasks (see results, paragraphs 3.3 – 3.5) and was the only parameter that classified the fluid reasoning tasks above chance using a multivariate approach (see results, paragraph 3.6), the coverage parameter was specifically used to be correlated with the fMRI data.

Coverage delta score of microstate A positively covaried with fMRI beta-values (SR – CC) during SR performance in medial posterior parietal cortex (BA 7; x = 0, y = -66, z = 56; 378 voxels), left pre-supplementary motor area (BA 6; x = -3, y = 13, z = 48; 297 voxels) and left superior frontal cortex (BA 8; x = -9, y = 28, z = 51; 378 voxels) ($r > 0.68$, $p < 0.01$ corrected, $k > 8$; see Figure 4).

Coverage delta score of microstate B covaried with fMRI beta-values (SR – CC or VZ – CC), negatively during SR performance in right hippocampus (BA 36; x = 21, y = -11, z = -19; 513 voxels) and left hippocampus (BA 36; x = -21, y = -11, z = -19; 378 voxels) ($r > -0.68$, $p < 0.01$ corrected, $k > 8$) and positively during VZ performance in medial (BA 18; x = 1, y = -61, z = 14; 243 voxels) and right inferior occipital cortex (BA 19; x = 30, y = -79, z = -11; 297 voxels) ($r > 0.68$, $p < 0.01$ corrected, $k > 8$; see Figure 4).

Coverage delta score of microstate C covaried with fMRI beta-values (SR – CC or VZ – CC), positively during SR performance in left hippocampus (BA 36; x = 21, y = -11, z = -19; 297 voxels) ($r > 0.68$, $p < 0.01$ corrected, $k > 8$) and negatively during VZ in right superior frontal cortex (BA 6; x = 9, y = 19, z = 55; 270 voxels) ($r > -0.68$, $p < 0.01$ corrected, $k > 8$; see Figure 4).

Coverage delta score of microstate D did not covary with fMRI beta-values (SR – CC) during SR performance.

Finally, average coverage delta score of microstate C (average IN/SR/VZ - CC) negatively covaried with average fMRI beta-values for the fluid intelligence tasks (average IN/SR/VZ - CC) in right medial superior frontal cortex (x = 8, y = 18, z = 55; 891 voxels) (BA 6; $r > -0.68$, $p < 0.01$ corrected, $k > 8$; see Figure 5).

4. Discussion

The present study aimed at investigating whether psychometrically distinct, but unidimensional, fluid reasoning processes, including induction, spatial relationships and visualization, could be differentiated by EEG microstate profiles. The results showed that microstate coverage as well as microstate duration were successful parameters in discriminating the fluid reasoning tasks (IN, SR, VZ) from a visuo-motor control task (CC). The coverage parameter showed the most variable pattern across the various fluid reasoning abilities and discriminated them most clearly. Specifically, we found the highest coverage of microstate B during both SR and VZ. By contrast, microstate C coverage was lowest during both SR and VZ. Moreover, coverage of microstate A was highest during SR, whereas coverage of microstate D was lowest during SR. Confirming the discriminative properties of the coverage parameter, multivariate classification analyses showed that only microstate coverage, but not the duration or occurrence parameters, was able to classify the different fluid reasoning tasks above chance.

4.1 Microstate coverage

Since coverage is calculated as the percentage of total recording time that the microstate is dominant during a certain condition (Lehmann, 1987; Lehmann & Koenig, 1997), it reflects the time coverage of a given microstate, compared to others, that is, it indicates the relative rather than absolute presence of a microstate. As a consequence, coverage differences between the fluid reason conditions could be interpreted to some degree as variations in the interdependency of microstates. This would be in line with the suggestion that individual microstate classes cannot be completely reduced to specific functions, but that they need to be viewed also in the context of their interplay to understand how they support specific cognitive processes (Milz et al., 2016). Supporting the view that global microstate features characterize different cognitive processes, multivariate classification analyses that examined the microstates together accurately classified the cognitively distinct fluid reasoning conditions. A different interplay between the microstates could be particularly relevant to characterize complex cognitive processes, like fluid reasoning abilities, that essentially rely on an integrative functioning of multiple brain networks (e.g. (Barbey et al., 2014; Burgaleta et al., 2014; Cole et al., 2015; Colom et al., 2006; Deary et al., 2010; Duncan, 2010; Ebisch et al., 2013; Gray et al., 2003; Roca et al., 2010; Roman et al., 2014; Santarnecchi & Pascual-Leone, 2017; Woolgar et al., 2010).

The results favour the interpretation that different fluid reasoning components can be distinguished by the coverage of certain microstate classes at the cost of other classes. Both SR and VZ showed the strongest modulations of coverage of microstates B and C, but the effects were opposite:

whereas microstate B coverage was enhanced, microstate C coverage was reduced during both SR and VZ. Furthermore, microstate D was increased and microstate A was decreased specifically during SR. Interestingly, SR and VZ have in common that they both emphasize visuospatial aspects of fluid reasoning. As also suggested by previous fMRI findings (Ebisch et al., 2013; Ebisch et al., 2012), SR and VZ put higher demands on visuospatial neural processes, compared to a stronger emphasis on abstract reasoning by IN. Because visual input was similar during all the conditions, it likely is the type of cognitive process, and not the physical stimulus property, that differentiates.

No consensus has been reached about the neural sources and functions related to each of the microstates, yet. However, several studies attempted to identify fMRI-based networks at rest as hemodynamic correlates of the various microstates. A combined EEG-fMRI study (Britz et al., 2010) associated microstate B with the posterior visual system, and microstate C with the salience network involved in interoception and task-level control. The salience network also has been found repeatedly involved in reasoning tasks (Crone et al., 2009; Ebisch et al., 2013; Ebisch et al., 2012; Hilger et al., 2017; Yuan et al., 2012). However, although the involvement of microstate B in visual processing has been confirmed by several studies (Michel & Koenig, 2017), the link between microstate C and the salience network remains more controversial. Indeed, other studies suggested that microstate C could be related to the default mode network composed of brain regions that are more active at rest (i.e. when not being involved in any particular cognitive task, but allowed to think freely) (see for review Michel & Koenig, 2017).

It can be argued that the observed reduction in microstate C coverage is more in line with a suppression of the task-negative default mode activity as commonly observed during cognitive task performance (Raichle et al., 2001; Shulman et al., 1997). Instead, in case of a task-positive network like the salience network activity, one would expect to see an increase in microstate C coverage. Accordingly, studies looking at microstates during task performance reported similar decreases in microstate C parameters during task, compared to rest (Milz et al., 2017; Seitzman et al., 2017). The microstate C reduction during fluid reasoning is partially in agreement with our hypothesis. A remaining question would be why this reduction was detected only during SR and VZ, but not IN, since all three conditions were cognitively demanding. One possible explanation is that microstate C does not reflect the default mode network generally, but that microstate classes represent specific components of this network (Milz et al., 2017). Evidence supporting our results of visuospatial specificity of microstate C reduction is provided by previous findings showing that this class indeed is more strongly decreased during visualization tasks, compared to a verbalization task (Milz et al., 2016).

The enhanced coverage of microstate B during SR and VZ confirms our hypothesis and is congruent with the visuospatial functions attributed to microstate B (Michel & Koenig, 2017). Indeed, electrical activity of left and right occipital cortices, including primary visual areas, have been associated with microstate B at rest (Custo et al., 2017). However, contrasting results have been described as well. For instance, decreases in microstate B were detected during a visualization task (Milz et al., 2016) due to a hypothesized relation between microstates and alpha inhibitory activity (Milz et al., 2017). A relevant detail that could explain this discrepancy is that, in Milz et al. (2016), participants were asked to internally visualize stimuli with their eyes closed. Differently, in our study, participants were required to perform cognitive operations on visually presented stimuli with their eyes open. Of interest, one study that investigated microstate modulations during task performance showed increased coverage and occurrence of microstate B in eyes open conditions, compared to eyes closed conditions (Seitzman et al., 2017).

Microstates thus seem to be modulated differently during eyes open and eyes closed conditions. It might further be speculated that this interacts with the task at hand. Seitzman and colleagues (2017)

did not find differences between rest and task conditions in microstate B parameters, neither during eyes closed nor during eyes open conditions, but this might not be surprising, given that their task (serial subtraction) was not very visually demanding. In our case, tasks that required explicit visuospatial processing and mental manipulation of direct visual input (SR and VZ, but not IN) enhanced microstate B. Hence, we propose that certain cognitive tasks can enhance microstate B coverage, especially when the task explicitly requires visuospatial reasoning in combination with direct visual input.

Finally, microstate A was decreased during SR and microstate D was increased during SR. Given that significant differences were found only for SR, these results did not confirm our expectations. Further studies would be needed to shed light on this task specificity. An association was reported of microstates A and D with the auditory network and the dorsal attention network (Britz et al., 2010), respectively. Whereas the former might be irrelevant for the fluid reasoning tasks, the latter plays a key role in spatial attention and working memory (Corbetta et al., 2002).

4.2 Microstate duration

Different from coverage, the duration of all four microstates was rather uniformly decreased during the various fluid reasoning tasks, compared to CC. In few cases, small, but significant differences were detected between the conditions suggesting a slightly stronger decrease of duration of microstates A and C during SR, and of microstate B during IN. In accordance with the uniform microstate duration profiles across the fluid reasoning conditions, multivariate analyses were not able to classify the conditions based on the duration parameter. The duration parameter is calculated as the average duration that a given microstate remains stable whenever it appears during the task trials (Lehmann & Koenig, 1997). As such, the microstate duration parameter could be interpreted as reflecting the stability of the activity of the microstate underlying neural assemblies. From this point of view, the consistent reduction of microstate duration during all the fluid reasoning conditions, compared to CC, could reflect a more dynamic state in which transitions from one microstate to another occur faster. Shorter microstate duration during task performance was also described by Seitzman et al. (2017) when comparing task with rest as well as when comparing eyes open with eyes closed conditions. Possibly, performance on tasks with higher cognitive demands requires to shift earlier from one microstate to another, compared to a spontaneous state or a task that is not particularly demanding.

To support this claim empirically, it would be necessary to study microstate parameters in relationship with varying levels of difficulty. Our experiment was not specifically designed for performing this analyses with optimal sensitivity, because fluid reasoning items with a medium difficulty level were selected for the EEG/fMRI study. Easy items were not included as they might not have been sufficiently demanding to neuro-functionally distinguish between the tasks that were cognitively highly similar, whereas difficult items were not included to avoid the risk that many trials needed to be excluded from the analyses due to incorrect responses by the participants. Another problem is that externally defined difficulty indices might not be fully generalizable to the context of EEG/fMRI measurements. Furthermore, previous studies reported inconsistent findings. Milz et al. (2016) showed decreases as well as increases of microstate duration during task performance, compared to rest, and decreases as well as increases of microstate duration were reported by Katayama et al. (2007) comparing rest and various levels of hypnosis. Future attempts are recommended to investigate if higher cognitive demands are associated with faster transitions between microstates by properly varying task difficulty.

4.3 BOLD covariance

Covariance with simultaneously recorded BOLD signal was preliminarily analysed to provide additional information about the brain processes associated with microstate parameters. In accordance with task-specific involvement of lower levels of processing (e.g. visual and perceptual stages) in fluid reasoning components (Brumback et al., 2004; Buschman et al., 2011; Ebisch et al., 2013; Melnick, Harrison et al., 2013; Narr et al., 2007; Soulieres et al., 2009) as well as with the supposed association between microstate B and the visual system (Custo et al., 2017; Michel & Koenig, 2017), this class positively correlated with BOLD response during VZ in visual occipital cortex. Confirming our hypothesis, the stronger individual coverage of microstate B, the stronger BOLD response in occipital cortex during VZ.

Differently, during SR microstate B negatively correlated with BOLD response in bilateral hippocampus. One possible interpretation of this unexpected result is that the hippocampus is part of the default mode network (Buckner et al., 2008), which is, as opposed to the visual network, a task negative network (Mayhew et al., 2013; Shulman et al., 1997). That is, the performance of demanding visual cognitive tasks could be accompanied by a suppression of activity in regions of the default mode network during those tasks (Mayhew et al., 2013; Uddin et al., 2009). Indeed, it needs to be reminded that the relations between EEG and fMRI data detected by covariance analysis are not necessarily direct and may reflect secondary neural processes, too. Moreover, some authors proposed that all microstates could be related to aspects of default mode network activity (Milz et al., 2017).

Hence, it can be considered an interesting finding that BOLD responses in hippocampus during SR also correlated with coverage of microstate C. Consistent with the positive correlation in this case, microstate C has been linked most directly with the default mode network (Michel & Koenig, 2017). Thus, the observed relations between BOLD and microstate parameters in hippocampus during SR could, directly (microstate C representing a task negative network) as well as indirectly (microstate B representing a task positive network inhibiting the task negative network), reflect modulations of the default mode during task performance.

Additional indications for a task negative network emerge when looking at the fMRI beta values in the hippocampus in the graphs of Figure 4. They appear to be mainly negative, meaning that hippocampus activity was weaker during SR, compared to CC. The negative relation between microstate C and BOLD response in supplementary motor area during SR could be interpreted in a similar way as microstate C and supplementary motor area are associated with task negative (default mode network) (Raichle et al., 2001) and relevant task positive networks (e.g. mental object rotation; Richter et al., 2000), respectively.

Nevertheless, alternative interpretations could apply to the observed link between the hippocampus and the SR task. For instance, studies reported that spatial aspects of intelligence (Colom et al., 2013) as well as other complex spatial cognitive functions (Buzsaki & Moser, 2013; O'keefe, 1978) also could be more directly related to the hippocampus. Interestingly, the relation between spatial intelligence and hippocampus properties was opposite in males and females (Colom et al., 2013) suggesting that mixed samples might also obscure links between brain and cognition. Since the present sample consisted of females only, it remains an open issue if the same or an opposite pattern is true for a male sample.

BOLD correlations of microstate A during SR are more difficult to interpret. Microstate A correlated positively with frontoparietal regions, including pre-supplementary motor cortex, medial superior frontal cortex and media superior parietal cortex. This seems in contrast with the link between microstate A and the auditory network (Britz et al., 2010), although Custo et al. (2017) reported additional sources of microstate A in frontal and motor cortex. Furthermore, similar

superior frontal and parietal regions were reported to be involved in the mental rotation of objects, an ability closely related to our SR task (Richter et al., 2000).

Finally, microstate classes were correlated with averaged BOLD responses during all the fluid reasoning tasks, that is, without differentiating between the conditions. In this case, only microstate C negatively covaried with BOLD response in medial superior frontal cortex. This region was found to be involved in fluid reasoning by a recent meta-analysis located in the dorsal attention network involved in executive control (Santarnecchi & Pascual-Leone, 2017). Because microstate C is presumed to reflect the default mode network as described above (Michel & Koenig, 2017), this negative correlation in medial superior frontal cortex could mean that lower default mode activity is inversely related to frontal attention network activity during fluid reasoning.

Although the investigation of the relationship between microstates and underlying brain network functions and sources using simultaneous EEG-fMRI data acquisition is an emerging topic, relatively few studies have been published at present to facilitate the interpretation of our findings. Few studies measured microstates during periods of cognitive task performance (Milz et al., 2016; Seitzman et al., 2017). The present study adds to this literature by showing how microstates can be specifically modulated by cognitively distinct fluid reasoning tasks and that they can be correlated with simultaneous BOLD responses.

4.4 Microstates and fluid reasoning

To our knowledge, only one previous study investigated the relationship between microstates and fluid reasoning (Santarnecchi et al., 2017). In their study, microstate parameters were calculated based on EEG recordings during a resting state. Confirming correlations between fMRI resting state networks and intelligence (Cole et al., 2015; Hilger et al., 2017; Santarnecchi et al., 2014; Song et al., 2008; van den Heuvel et al., 2009), correlations were detected between fluid reasoning performance and EEG microstate B and C parameters in the brain at rest. Given that we calculated microstate parameters during task performance, their results might not be directly comparable with ours. Nevertheless, it is remarkable that microstates B and C also could be related to fluid reasoning components in our study as they appeared to be specifically modulated during fluid reasoning tasks that emphasized visuospatial processing.

No specific microstate modulation was detected for IN representing a more abstract reasoning task. While IN did not modulate microstate coverage, it generally did modulate microstate duration in a similar way as SR and VZ, compared to CC. Only microstate B duration was slightly more reduced during IN, compared to VZ, but not compared to SR. Considering this pattern of results, we propose that the four microstates could be more sensitive to tasks that strongly rely on the sensory and cognitive processing of low level (visual) input. Relevantly, Santarnecchi and colleagues (2017) also reported different microstate classes being linked with distinct fluid reasoning tasks. Because few studies analysed microstates during task performance (e.g. Milz et al., 2016; Seitzman et al., 2017), the relationships between cognitive functions, and rest and task conditions remain a relevant topic for future investigations.

4.5 Limitations

Some limitations need to be mentioned. Firstly, further studies are urged not only to identify the functional and anatomical correlates of the microstate classes, but also to clarify the specific meaning and interpretation of their related parameters (coverage, duration and occurrence). Indeed, the behaviour of such parameters is not fully congruent across studies. Moreover, only very few studies reported results about microstate modulations during tasks. To our knowledge, all the

studies that aimed to determine the brain networks underlying microstates, both directly from EEG data (Custo et al., 2017; Milz et al., 2017; Pascual-Marqui et al., 2014) and in association with fMRI (Britz et al., 2010; Musso et al., 2010; Yuan et al., 2012), are resting-state studies.

Secondly, other areas beyond those associated with the canonical four microstates could be recruited when performing a complex task. A possible improvement of our approach could be to consider more than four microstates. Here, we applied the Krzanowski-Lai criterion to our data to choose four as optimal number of microstates. The 4 canonical classes explained about 75% of the variance of our EEG data.

Thirdly, reproducibility is an important issue to consider, especially in the context of a relatively limited sample size. In the present study two procedures were adapted to address this issue and provide some information about the reliability of the results. We calculated 95% CIs providing information about the range of the population mean estimates as well as the precision of these estimates. As such, CIs are related to replicability and generalizability. Relatively narrow and non-overlapping 95% CIs for the fluid reasoning conditions for the coverage parameter suggest that the detected differences in the sample mean between the conditions are rather robust with a probability of being caused by a sampling error below five percent. Moreover, multivariate classification analyses were performed on the single trial/subject level using a leave-one-out cross-validation procedure. At each cross-validation step, the classifier was trained with all the single trials of 19 subjects and tested with all the single trials of the excluded subject. This procedure yielded an above chance classification performance. Although the CIs and the multivariate classification results support an adequate replicability and generalizability of the study results, representing promising future directions, replication studies in separate datasets as well as analyses of correlations with differences in behavioral performance in a large cohort would be needed to enforce these claims.

Finally, the interpretation of correlations between fMRI and EEG data is not always unequivocal. In the present study, we chose to preliminarily correlate average microstate parameters with average BOLD responses across conditions and individuals. It has been argued that larger samples are needed to obtain stable correlation estimates (Schönbrodt and Perugini, 2013), and the EEG-fMRI correlations also might reflect indirect relationships, such as the suppression of activity in task-irrelevant networks by activity in task-relevant networks. Moreover, the relationships between excitatory and inhibitory processes and how they affect microstates are still issues of debate (Milz et al., 2017). In fact, EEG data are band-pass filtered from 1 to 30 Hz and in this range, the frequency band with the strongest power is the alpha band. The functional significance of this rhythm is still a matter of debate. Dependently on the sub-frequency range (high alpha or low alpha), the cortical source and the specific task, alpha rhythm can exhibit active inhibitory functions (Klimesch, 2012). The integration of microstate parameters with BOLD signals has been rarely investigated (Britz et al., 2010; Musso et al., 2010), and only during a resting state characterized by ongoing BOLD signal fluctuations. New studies need develop more sophisticated methods to allow the integration of EEG microstates with the BOLD signal by exploiting within subject temporal variability during performance on randomized task conditions.

4.6 Conclusion

The present study investigated microstates during different fluid reasoning tasks. In agreement with psychometric models of cognitive abilities (Carroll, 1993; Colom et al., 2006; Colom et al., 2010; Roman et al., 2014), and expanding previous fMRI results (Ebisch et al., 2013; Ebisch et al., 2012), the findings show that unidimensional cognitive abilities, such as IN, SR and VZ, are distinguishable at the neuro-functional level as indicated by EEG microstate parameters. Changes in

microstates, reflecting the topography of global field power, indicate changes in the global coordination of neuronal activity over time (Khanna et al., 2015; Lehmann & Koenig, 1997; Lehmann & Michel, 2011). The observed differences in microstate parameters thus could be interpreted in terms of a different interplay between brain networks during distinct, but unidimensional, fluid reasoning abilities.

In the present context, such brain networks seem to be especially related to visuospatial processing. Whereas previous studies showed specific neural correlates of IN and VZ in fMRI data (Ebisch et al., 2012), in the present study, using simultaneously acquired EEG data, SR showed the most distinctive activity pattern. In conclusion, microstates could add valuable information about how brain function supports fluid reasoning with increased sensitivity in the temporal domain. This complementary role of microstates might be due to the fact that fMRI and EEG reflect partially distinct neurophysiological processes, and because of the higher temporal resolution of EEG allowing to detect processes (e.g. microstates) with a dynamic temporal structure during complex tasks.

Declarations of interest: The authors do not declare any conflict of interest. This research did not receive any specific grant from funding agencies in the public, commercial, or not-for-profit sectors.

5. References

Alexander, G. E., Furey, M. L., Grady, C. L., Pietrini, P., Brady, D. R., Mentis, M. J., & Schapiro, M. B. (1997). Association of premorbid intellectual function with cerebral metabolism in Alzheimer's disease: implications for the cognitive reserve hypothesis. *Am J Psychiatry, 154*(2), 165-172. doi:10.1176/ajp.154.2.165

Allen, P. J., Josephs, O., & Turner, R. (2000). A method for removing imaging artifact from continuous EEG recorded during functional MRI. *Neuroimage, 12*(2), 230-239. doi:10.1006/nimg.2000.0599

Barbey, A. K., Colom, R., Paul, E. J., & Grafman, J. (2014). Architecture of fluid intelligence and working memory revealed by lesion mapping. *Brain Struct Funct, 219*(2), 485-494. doi:10.1007/s00429-013-0512-z

Barbey, A. K., Colom, R., Solomon, J., Krueger, F., Forbes, C., & Grafman, J. (2012). An integrative architecture for general intelligence and executive function revealed by lesion mapping. *Brain, 135*(Pt 4), 1154-1164. doi:10.1093/brain/aws021

Basten, U. H., K.; Fiebach, C.J. (2015). Where smart brains are different: A quantitative meta-analysis of functional and structural brain imaging studies on intelligence. *Intelligence, 51*, 10-27.

Batty, G. D., Deary, I. J., & Gottfredson, L. S. (2007). Premorbid (early life) IQ and later mortality risk: systematic review. *Ann Epidemiol, 17*(4), 278-288. doi:10.1016/j.annepidem.2006.07.010

Bock, R. D. (1997). A brief history of item response theory. *Educ. Meas., Issues Pract., 16*, 21-33.

Britz, J., Van De Ville, D., & Michel, C. M. (2010). BOLD correlates of EEG topography reveal rapid resting-state network dynamics. *Neuroimage, 52*(4), 1162-1170. doi:10.1016/j.neuroimage.2010.02.052

Brodbeck, V., Kuhn, A., von Wegner, F., Morzelewski, A., Tagliazucchi, E., Borisov, S., . . . Laufs, H. (2012). EEG microstates of wakefulness and NREM sleep. *Neuroimage, 62*(3), 2129-2139. doi:10.1016/j.neuroimage.2012.05.060

Brumback, C. R., Low, K. A., Gratton, G., & Fabiani, M. (2004). Sensory ERPs predict differences in working memory span and fluid intelligence. *Neuroreport, 15*(2), 373-376.

Brunet, D., Murray, M. M., & Michel, C. M. (2011). Spatiotemporal analysis of multichannel EEG: CARTOOL. *Comput Intell Neurosci, 2011*, 813870. doi:10.1155/2011/813870

Buckley, J., Seery, N., Canty, D., & Gumaelius, L. (2018). Visualization, inductive reasoning, and memory span as components of fluid intelligence: Implications for technology education. *International Journal of Educational Research, 90*, 64-77. doi: 10.1016/j.ijer.2018.05.007

Buckner, R. L., Andrews-Hanna, J. R., & Schacter, D. L. (2008). The brain's default network: anatomy, function, and relevance to disease. *Ann N Y Acad Sci, 1124*, 1-38. doi:10.1196/annals.1440.011

Burgaleta, M., MacDonald, P. A., Martinez, K., Roman, F. J., Alvarez-Linera, J., Ramos Gonzalez, A., . . . Colom, R. (2014). Subcortical regional morphology correlates with fluid and spatial intelligence. *Hum Brain Mapp, 35*(5), 1957-1968. doi:10.1002/hbm.22305

Burgess, G. C., Gray, J. R., Conway, A. R., & Braver, T. S. (2011). Neural mechanisms of interference control underlie the relationship between fluid intelligence and working memory span. *J Exp Psychol Gen, 140*(4), 674-692. doi:10.1037/a0024695

Buschman, T. J., Siegel, M., Roy, J. E., & Miller, E. K. (2011). Neural substrates of cognitive capacity limitations. *Proc Natl Acad Sci U S A, 108*(27), 11252-11255. doi:10.1073/pnas.1104666108

Buzsaki, G., & Moser, E. I. (2013). Memory, navigation and theta rhythm in the hippocampal-entorhinal system. *Nat Neurosci, 16*(2), 130-138. doi:10.1038/nn.3304

Calvin, C. M., Batty, G. D., Der, G., Brett, C. E., Taylor, A., Pattie, A., . . . Deary, I. J. (2017). Childhood intelligence in relation to major causes of death in 68 year follow-up: prospective population study. *BMJ, 357*, j2708. doi:10.1136/bmj.j2708

Calvin, C. M., Deary, I. J., Fenton, C., Roberts, B. A., Der, G., Leckenby, N., & Batty, G. D. (2011). Intelligence in youth and all-cause-mortality: systematic review with meta-analysis. *Int J Epidemiol, 40*(3), 626-644. doi:10.1093/ije/dyq190

Cawley, G.C., Talbot, N.L.C. (2004). Fast exact leave-one-out cross-validation of sparse least-squares support vector machines. *Neural Networks, 17*, 1467–1475. https://doi.org/10.1016/j.neunet.2004.07.002

Carroll, J. (1993). *Human Cognitive Abilities: A Survey of Factor-Analytic Studies*: Cambridge University Press, Cambridge, UK.

Cattell, R. B. (1963). Theory of fluid and crystallized intelligence: a critical experiment. *Journal of Educational Psychology, 54*, 1-22.

Cattell, R. B. (1987). *Intelligence: Its Structure, Growth and Action*: North-Holland.

Cole, M. W., Ito, T., & Braver, T. S. (2015). Lateral Prefrontal Cortex Contributes to Fluid Intelligence Through Multinetwork Connectivity. *Brain Connect, 5*(8), 497-504. doi:10.1089/brain.2015.0357

Colom, R., Burgaleta, M., Roman, F. J., Karama, S., Alvarez-Linera, J., Abad, F. J., . . . Haier, R. J. (2013). Neuroanatomic overlap between intelligence and cognitive factors: morphometry methods provide support for the key role of the frontal lobes. *Neuroimage, 72*, 143-152. doi:10.1016/j.neuroimage.2013.01.032

Colom, R., Jung, R. E., & Haier, R. J. (2006). Distributed brain sites for the g-factor of intelligence. *Neuroimage, 31*(3), 1359-1365. doi:10.1016/j.neuroimage.2006.01.006

Colom, R., Karama, S., Jung, R. E., & Haier, R. J. (2010). Human intelligence and brain networks. *Dialogues Clin Neurosci, 12*(4), 489-501.

Colom, R., & Quiroga, M. A. (2009). Neuroticism, intelligence, and intra-individual variability in elementary cognitive tasks: testing the mental noise hypothesis. *Psicothema, 21*(3), 403-408.

Colom, R., Stein, J. L., Rajagopalan, P., Martinez, K., Hermel, D., Wang, Y., . . . Thompson, P. M. (2013). Hippocampal structure and human cognition: key role of spatial processing and

evidence supporting the efficiency hypothesis in females. *Intelligence, 41*(2), 129-140. doi:10.1016/j.intell.2013.01.002

Comon, P. (1994). Independent component analysis—A new concept? *Signal Process, 36*, 287–314.

Corbetta, M., Kincade, J. M., & Shulman, G. L. (2002). Neural systems for visual orienting and their relationships to spatial working memory. *J Cogn Neurosci, 14*(3), 508-523. doi:10.1162/089892902317362029

Cortes, C., Vapnik, V. (1995). Support-vector networks. *Mach Learn 20*, 273–297. https://doi.org/10.1007/BF00994018

Cox, R. W. (1996). AFNI: Software for analysis and visualization of functional magnetic resonance neuroimages. Computers and Biomedical Research, 29, 162–173.

Crone, E. A., Wendelken, C., van Leijenhorst, L., Honomichl, R. D., Christoff, K., & Bunge, S. A. (2009). Neurocognitive development of relational reasoning. *Dev Sci, 12*(1), 55-66. doi:10.1111/j.1467-7687.2008.00743.x

Custo, A., Van De Ville, D., Wells, W. M., Tomescu, M. I., Brunet, D., & Michel, C. M. (2017). Electroencephalographic Resting-State Networks: Source Localization of Microstates. *Brain Connect, 7*(10), 671-682. doi:10.1089/brain.2016.0476

Deary, I. J., Batty, D., & Gottfredson, L. S. (2005). Human hierarchies, health, and IQ. *Science, 309*(5735), 703; author reply 703. doi:10.1126/science.309.5735.703

Deary, I. J., Penke, L., & Johnson, W. (2010). The neuroscience of human intelligence differences. *Nat Rev Neurosci, 11*(3), 201-211. doi:10.1038/nrn2793

Duncan, J. (2010). The multiple-demand (MD) system of the primate brain: mental programs for intelligent behaviour. *Trends Cogn Sci, 14*(4), 172-179. doi:10.1016/j.tics.2010.01.004

Duncan, J., Burgess, P., & Emslie, H. (1995). Fluid intelligence after frontal lobe lesions. *Neuropsychologia, 33*(3), 261-268.

Duncan, J., Seitz, R. J., Kolodny, J., Bor, D., Herzog, H., Ahmed, A., . . . Emslie, H. (2000). A neural basis for general intelligence. *Science, 289*(5478), 457-460.

Ebisch, S. J., Mantini, D., Romanelli, R., Tommasi, M., Perrucci, M. G., Romani, G. L., . . . Saggino, A. (2013). Long-range functional interactions of anterior insula and medial frontal cortex are differently modulated by visuospatial and inductive reasoning tasks. *Neuroimage, 78*, 426-438. doi:10.1016/j.neuroimage.2013.04.058

Ebisch, S. J., Perrucci, M. G., Mercuri, P., Romanelli, R., Mantini, D., Romani, G. L., . . . Saggino, A. (2012). Common and unique neuro-functional basis of induction, visualization, and spatial relationships as cognitive components of fluid intelligence. *Neuroimage, 62*(1), 331-342. doi:10.1016/j.neuroimage.2012.04.053

Embreston, S. E. R., S.P. (2000). *Item Response Theory for Psychologists*: Lawrence Erlbaunm Associates Publishers, Mahwah, New Jersey, London

Forman, S. D., Cohen, J. D., Fitzgerald, M., Eddy, W. F., Mintun, M. A., & Noll, D. C. (1995). Improved assessment of significant activation in functional magnetic resonance imaging (fMRI): use of a cluster-size threshold. *Magn Reson Med, 33*(5), 636-647.

Gazzaley, A., Cooney, J. W., Rissman, J., & D'Esposito, M. (2005). Top-down suppression deficit underlies working memory impairment in normal aging. *Nat Neurosci, 8*(10), 1298-1300. doi:10.1038/nn1543

Glascher, J., Rudrauf, D., Colom, R., Paul, L. K., Tranel, D., Damasio, H., & Adolphs, R. (2010). Distributed neural system for general intelligence revealed by lesion mapping. *Proc Natl Acad Sci U S A, 107*(10), 4705-4709. doi:10.1073/pnas.0910397107

Glascher, J., Tranel, D., Paul, L. K., Rudrauf, D., Rorden, C., Hornaday, A., . . . Adolphs, R. (2009). Lesion mapping of cognitive abilities linked to intelligence. *Neuron, 61*(5), 681-691. doi:10.1016/j.neuron.2009.01.026

Gottfredson, L. S. (1997). Why g matters: the complexity of everyday life. *Intelligence, 24*, 79-132.

Gray, J. R., Chabris, C. F., & Braver, T. S. (2003). Neural mechanisms of general fluid intelligence. *Nat Neurosci, 6*(3), 316-322. doi:10.1038/nn1014

Gray, J. R., & Thompson, P. M. (2004). Neurobiology of intelligence: Health implications? *Discov Med, 4*(22), 157-162.

Hayes, T. R. P., A.A.; Sederberg, P.B. (2015). Do we really become smarter when our fluid intelligence test scores improve? *Intelligence, 48*, 1-14.

Hilger, K., Ekman, M., Fiebach, C. J., & Basten, U. (2017). Intelligence is associated with the modular structure of intrinsic brain networks. *Sci Rep, 7*(1), 16088. doi:10.1038/s41598-017-15795-7

Hossiep, R. T., D.; Hasella, M. (1999). *Bochumer Matrizentest (BOMAT) Advanced*: Hogrefe.

Hunt, E. B. (2011). *Human Intelligence*: Cambridge University Press, Cambridge, UK.

Hyvärinen, A. K., J.; Oja, E. (2001). *Independent Component Analysis*: John Wiley and Sons, New York.

James, C. J. H., C.W. (2004). Independent component analysis for biomedical signals. *Physiological Measurements, 26*(R15–R39).

Jensen, A. R. (1980). *Bias in Mental Testing*: Free, New York.

Jensen, A. R. (1998). *The g Factor*: Praeger, Westport, CT.

Jung, R. E., & Haier, R. J. (2007). The Parieto-Frontal Integration Theory (P-FIT) of intelligence: converging neuroimaging evidence. *Behav Brain Sci, 30*(2), 135-154; discussion 154-187. doi:10.1017/S0140525X07001185

Katayama, H., Gianotti, L. R., Isotani, T., Faber, P. L., Sasada, K., Kinoshita, T., & Lehmann, D. (2007). Classes of multichannel EEG microstates in light and deep hypnotic conditions. *Brain topography, 20(1)*, 7-14. doi: 10.1007/s10548-007-0024-3

Khanna, A., Pascual-Leone, A., Michel, C. M., & Farzan, F. (2015). Microstates in resting-state EEG: current status and future directions. *Neurosci Biobehav Rev, 49*, 105-113. doi:10.1016/j.neubiorev.2014.12.010

Klimesch, W. (2012). alpha-band oscillations, attention, and controlled access to stored information. *Trends Cogn Sci, 16*(12), 606-617. doi:10.1016/j.tics.2012.10.007

Koenig, T., Lehmann, D., Merlo, M. C., Kochi, K., Hell, D., & Koukkou, M. (1999). A deviant EEG brain microstate in acute, neuroleptic-naive schizophrenics at rest. *Eur Arch Psychiatry Clin Neurosci, 249*(4), 205-211.

Lee, K. H., Choi, Y. Y., Gray, J. R., Cho, S. H., Chae, J. H., Lee, S., & Kim, K. (2006). Neural correlates of superior intelligence: stronger recruitment of posterior parietal cortex. *Neuroimage, 29*(2), 578-586. doi:10.1016/j.neuroimage.2005.07.036

Lehmann, D. (1987). Principles of spatial analysis. In A. S. R. Gevins, A. (Ed.), *Methods of analysis of brain electrical and magnetic signals* (pp. 309-354): Elsevier, Amsterdam.

Lehmann, D., & Koenig, T. (1997). Spatio-temporal dynamics of alpha brain electric fields, and cognitive modes. *Int J Psychophysiol, 26*(1-3), 99-112.

Lehmann, D., & Michel, C. M. (2011). EEG-defined functional microstates as basic building blocks of mental processes. *Clin Neurophysiol, 122*(6), 1073-1074. doi:10.1016/j.clinph.2010.11.003

Lopes da Silva, F. H. (1991). Neural mechanisms underlying brain waves: from neural membranes to networks. *Electroencephalography in Clinical Neurophysiology*(79), 81-93.

Lopes da Silva, F. H. V. R., A. (2012). Biophysical aspects of EEG and Magnetoencephalogram generation. In D. L. L. d. S. Scho, F.H. (Ed.), *Niedermeyer's Electroencephalography*: Lippincott Williams and Wilkins, Wolters Kluwer, Philadelphia.

Mantini, D., Perrucci, M. G., Cugini, S., Ferretti, A., Romani, G. L., & Del Gratta, C. (2007). Complete artifact removal for EEG recorded during continuous fMRI using independent component analysis. *Neuroimage, 34*(2), 598-607. doi:10.1016/j.neuroimage.2006.09.037

Matsuda, O., & Saito, M. (1998). Crystallized and fluid intelligence in elderly patients with mild dementia of the Alzheimer type. *Int Psychogeriatr, 10*(2), 147-154.

Matzen, L. E. B., Z.O.; Dixon, K.R.; Posey, J.; Kroger, J.K.; Speed, A.E. (2010). Recreating Raven's: Software for systematically generating large numbers of Raven-like matrix problems with normed properties. *Behavior research methods, 42*, 525-541.

Mayhew, S. D., Ostwald, D., Porcaro, C., & Bagshaw, A. P. (2013). Spontaneous EEG alpha oscillation interacts with positive and negative BOLD responses in the visual-auditory cortices and default-mode network. *Neuroimage, 76*, 362-372. doi:10.1016/j.neuroimage.2013.02.070

Melnick, M. D., Harrison, B. R., Park, S., Bennetto, L., & Tadin, D. (2013). A strong interactive link between sensory discriminations and intelligence. *Curr Biol, 23*(11), 1013-1017. doi:10.1016/j.cub.2013.04.053

Michel, C. M., & Koenig, T. (2017). EEG microstates as a tool for studying the temporal dynamics of whole-brain neuronal networks: A review. *Neuroimage*. doi:10.1016/j.neuroimage.2017.11.062

Milz, P., Faber, P. L., Lehmann, D., Koenig, T., Kochi, K., & Pascual-Marqui, R. D. (2016). The functional significance of EEG microstates--Associations with modalities of thinking. *Neuroimage, 125*, 643-656. doi:10.1016/j.neuroimage.2015.08.023

Milz, P., Pascual-Marqui, R. D., Achermann, P., Kochi, K., & Faber, P. L. (2017). The EEG microstate topography is predominantly determined by intracortical sources in the alpha band. *Neuroimage, 162*, 353-361. doi:10.1016/j.neuroimage.2017.08.058

Murray, M. M., Brunet, D., & Michel, C. M. (2008). Topographic ERP analyses: a step-by-step tutorial review. *Brain Topogr, 20*(4), 249-264. doi:10.1007/s10548-008-0054-5

Musso, F., Brinkmeyer, J., Mobascher, A., Warbrick, T., & Winterer, G. (2010). Spontaneous brain activity and EEG microstates. A novel EEG/fMRI analysis approach to explore resting-state networks. *Neuroimage, 52*(4), 1149-1161. doi:10.1016/j.neuroimage.2010.01.093

Muthukrishnan, S.-P., Ahuja, N., Mehta, N., & Sharma, R. (2016). Functional brain microstate predicts the outcome in a visuospatial working memory task. *Behavioural brain research, 314*, 134-142. doi: 10.1016/j.bbr.2016.08.020

Narr, K. L., Woods, R. P., Thompson, P. M., Szeszko, P., Robinson, D., Dimtcheva, T., . . . Bilder, R. M. (2007). Relationships between IQ and regional cortical gray matter thickness in healthy adults. *Cereb Cortex, 17*(9), 2163-2171. doi:10.1093/cercor/bhl125

O'keefe, J. N., L. (1978). *The hippocampus as a cognitive map*: Oxford: Clarendon Press.

Pascual-Marqui, R. D., Michel, C. M., & Lehmann, D. (1995). Segmentation of brain electrical activity into microstates: model estimation and validation. *IEEE Trans Biomed Eng, 42*(7), 658-665. doi:10.1109/10.391164

Pascual-Marqui, R. D. L., D.; Faber, P.; Milz, P.; Kochi, K.; Yoshimura, M.; Nishida, K.; Isotani, T; Kinoshita, T. (2014). The resting microstate networks (RMN): cortical distributions, dynamics, and frequency specific information flow. *arXiv.org > q-bio > arXiv:1411.1949*.

Perfetti, B., Saggino, A., Ferretti, A., Caulo, M., Romani, G. L., & Onofrj, M. (2009). Differential patterns of cortical activation as a function of fluid reasoning complexity. *Hum Brain Mapp, 30*(2), 497-510. doi:10.1002/hbm.20519

Prabhakaran, V., Smith, J. A., Desmond, J. E., Glover, G. H., & Gabrieli, J. D. (1997). Neural substrates of fluid reasoning: an fMRI study of neocortical activation during performance of the Raven's Progressive Matrices Test. *Cogn Psychol, 33*(1), 43-63. doi:10.1006/cogp.1997.0659

Raichle, M. E., MacLeod, A. M., Snyder, A. Z., Powers, W. J., Gusnard, D. A., & Shulman, G. L. (2001). A default mode of brain function. *Proc Natl Acad Sci U S A, 98*(2), 676-682. doi:10.1073/pnas.98.2.676

Raven, J. (2003). Raven progressive matrices. In *Handbook of nonverbal assessment* (pp. 223-237): Springer, Boston, MA.

1211 Richter, W., Somorjai, R., Summers, R., Jarmasz, M., Menon, R. S., Gati, J. S., . . . Kim, S. G.
1212 (2000). Motor area activity during mental rotation studied by time-resolved single-trial
1213 fMRI. *J Cogn Neurosci, 12*(2), 310-320.
1214 Rifkin, R., Klautau, A. (2004). In Defense of One-Vs-All Classification. *Journal of Machine*
1215 *Learning Research, 5*, 101–141.
1216 Roca, M., Parr, A., Thompson, R., Woolgar, A., Torralva, T., Antoun, N., . . . Duncan, J. (2010).
1217 Executive function and fluid intelligence after frontal lobe lesions. *Brain, 133*(Pt 1), 234-
1218 247. doi:10.1093/brain/awp269
1219 Roman, F. J., Abad, F. J., Escorial, S., Burgaleta, M., Martinez, K., Alvarez-Linera, J., . . . Colom,
1220 R. (2014). Reversed hierarchy in the brain for general and specific cognitive abilities: a
1221 morphometric analysis. *Hum Brain Mapp, 35*(8), 3805-3818. doi:10.1002/hbm.22438
1222 Romanelli, R. S., A. (2014). *FIT- Fluid Intelligence Test Manuale*: Hogrefe Editore, Firenze.
1223 Santarnecchi, E., Galli, G., Polizzotto, N. R., Rossi, A., & Rossi, S. (2014). Efficiency of weak
1224 brain connections support general cognitive functioning. *Hum Brain Mapp, 35*(9), 4566-
1225 4582. doi:10.1002/hbm.22495
1226 Santarnecchi, E., Khanna, A. R., Musaeus, C. S., Benwell, C. S. Y., Davila, P., Farzan, F., . . .
1227 Honeywell, S. T. a. (2017). EEG Microstate Correlates of Fluid Intelligence and Response
1228 to Cognitive Training. *Brain Topogr, 30*(4), 502-520. doi:10.1007/s10548-017-0565-z
1229 Santarnecchi, E., Tatti, E., Rossi, S., Serino, V., & Rossi, A. (2015). Intelligence-related differences
1230 in the asymmetry of spontaneous cerebral activity. *Hum Brain Mapp, 36*(9), 3586-3602.
1231 doi:10.1002/hbm.22864
1232 Santarnecchi, E. E., A.; Pascual-Leone, A. . (2017). Dissecting the parieto-frontal correlates of fluid
1233 intelligence: A comprehensive ALE meta-analysis study. *Intelligence, 63*, 9-28.
1234 Schönbrodt, F. D., & Perugini, M. (2013). At what sample size do correlations stabilize? Journal of
1235 Research in Personality, 47(5), 609-612. doi: 10.1016/j.jrp.2013.05.009
1236 Seitzman, B. A., Abell, M., Bartley, S. C., Erickson, M. A., Bolbecker, A. R., & Hetrick, W. P.
1237 (2017). Cognitive manipulation of brain electric microstates. *Neuroimage, 146*, 533-543.
1238 doi:10.1016/j.neuroimage.2016.10.002
1239 Shulman, G. L., Fiez, J. A., Corbetta, M., Buckner, R. L., Miezin, F. M., Raichle, M. E., &
1240 Petersen, S. E. (1997). Common Blood Flow Changes across Visual Tasks: II. Decreases in
1241 Cerebral Cortex. *J Cogn Neurosci, 9*(5), 648-663. doi:10.1162/jocn.1997.9.5.648
1242 Song, M., Zhou, Y., Li, J., Liu, Y., Tian, L., Yu, C., & Jiang, T. (2008). Brain spontaneous
1243 functional connectivity and intelligence. *Neuroimage, 41*(3), 1168-1176.
1244 doi:10.1016/j.neuroimage.2008.02.036
1245 Soulieres, I., Dawson, M., Samson, F., Barbeau, E. B., Sahyoun, C. P., Strangman, G. E., . . .
1246 Mottron, L. (2009). Enhanced visual processing contributes to matrix reasoning in autism.
1247 *Hum Brain Mapp, 30*(12), 4082-4107. doi:10.1002/hbm.20831
1248 Spearman, C. (1927). *The Abilities of Man: Their Nature and Measurement*: Macmillan, New York
1249 (NY).
1250 Uddin, L. Q., Kelly, A. M., Biswal, B. B., Castellanos, F. X., & Milham, M. P. (2009). Functional
1251 connectivity of default mode network components: correlation, anticorrelation, and
1252 causality. *Hum Brain Mapp, 30*(2), 625-637. doi:10.1002/hbm.20531
1253 van den Heuvel, M. P., Stam, C. J., Kahn, R. S., & Hulshoff Pol, H. E. (2009). Efficiency of
1254 functional brain networks and intellectual performance. *J Neurosci, 29*(23), 7619-7624.
1255 doi:10.1523/JNEUROSCI.1443-09.2009
1256 Vanderperren, K., De Vos, M., Ramautar, J. R., Novitskiy, N., Mennes, M., Assecondi, S., . . . Van
1257 Huffel, S. (2010). Removal of BCG artifacts from EEG recordings inside the MR scanner: a
1258 comparison of methodological and validation-related aspects. *Neuroimage, 50*(3), 920-934.
1259 doi:10.1016/j.neuroimage.2010.01.010

Whalley, L. J., Deary, I. J., Appleton, C. L., & Starr, J. M. (2004). Cognitive reserve and the neurobiology of cognitive aging. *Ageing Res Rev, 3*(4), 369-382. doi:10.1016/j.arr.2004.05.001

Woolgar, A., Parr, A., Cusack, R., Thompson, R., Nimmo-Smith, I., Torralva, T., . . . Duncan, J. (2010). Fluid intelligence loss linked to restricted regions of damage within frontal and parietal cortex. *Proc Natl Acad Sci U S A, 107*(33), 14899-14902. doi:10.1073/pnas.1007928107

Yuan, Z., Qin, W., Wang, D., Jiang, T., Zhang, Y., & Yu, C. (2012). The salience network contributes to an individual's fluid reasoning capacity. *Behav Brain Res, 229*(2), 384-390. doi:10.1016/j.bbr.2012.01.037

Figure 1. Graphic representation of the microstate analysis procedure. On EEG trials with successful responses Global Field Power (GFP) curve (in black) is calculated. The topographies corresponding to the local maxima of GFP are then submitted to the modified version of k-mean clustering algorithm. This step provides four maps for each subject and each condition (CC, IN, RS, VZ). A second pseudo-clustering procedure was applied to obtain four global group templates. To describe the original EEG signals as a sequence of microstates, the original maps at GFP maxima are labelled on the basis of the maximal spatial correlation with the group template.

Figure 2. (A) Topographic maps of the four microstates (A, B, C, D) detected during the experimental tasks SR, VZ, IN, CC; (B) Bar graphs showing microstate coverage (average % ± S.E.) and differences between the conditions (black bars indicate significant differences compared to CC based on one sample t-tests; asterisks indicate differences between the conditions SR, VZ and IN based on paired sample t-tests); (C) Bar graphs showing microstate durations (average ms ± S.E.) and differences between the conditions (red dots indicate significant differences compared to CC based on one sample t-tests; asterisks indicate differences between the conditions SR, VZ and IN based on paired sample t-tests).

Figure 3. Confusion matrix of the classification results. The predicted class, i.e. the output of classification, are on the rows and the true classes on the columns. The matrix shows the percentage of classification: only the values on the diagonal express correct classification (predicted class is classified as the true class), while extra-diagonal values the percentage of un-correct classifications (predicted class is not classified as the true class). To be noted that the sum of the values in each column is equal to 100%, the sum of the correct (diagonal) and un-correct (extra-diagonal) classifications for the corresponding true class.

Figure 4. Brain clusters characterized by a significant correlation between BOLD response and microstate coverage during the different fluid reasoning tasks (delta's relative to CC). Scatterplots illustrate the distribution of BOLD response delta's and microstate coverage delta's as well as their relationship ($r > |0.68|$).

Figure 5. Brain clusters characterized by a significant correlation between BOLD response and microstate coverage during the averaged fluid reasoning tasks (delta's relative to CC). Scatterplots illustrate the distribution of BOLD response delta's and microstate coverage delta's as well as their relationship ($r > -0.68$).

Table 1. Difficulty of the selected items for the different Gf conditions used for the fMRI-EEG experiment according to IRT parameter *a* (difficulty; mean Logit ± standard deviation).

Induction	**Visualization**	**Spatial relationships**
− 0.82 ± 0.95	− 0.82 ± 0.93	− 0.82 ± 0.96

Table 2. Behavioral results: reaction times (RT in ms) and errors (%)

	RT *Mean ± SD*	**Errors** *Mean ± SD*
Induction	15922 ± 4520	25 ± 14
Spatial Relationships	15297 ± 4715	22 ± 19
Visualization	14863 ± 4440	27 ± 14

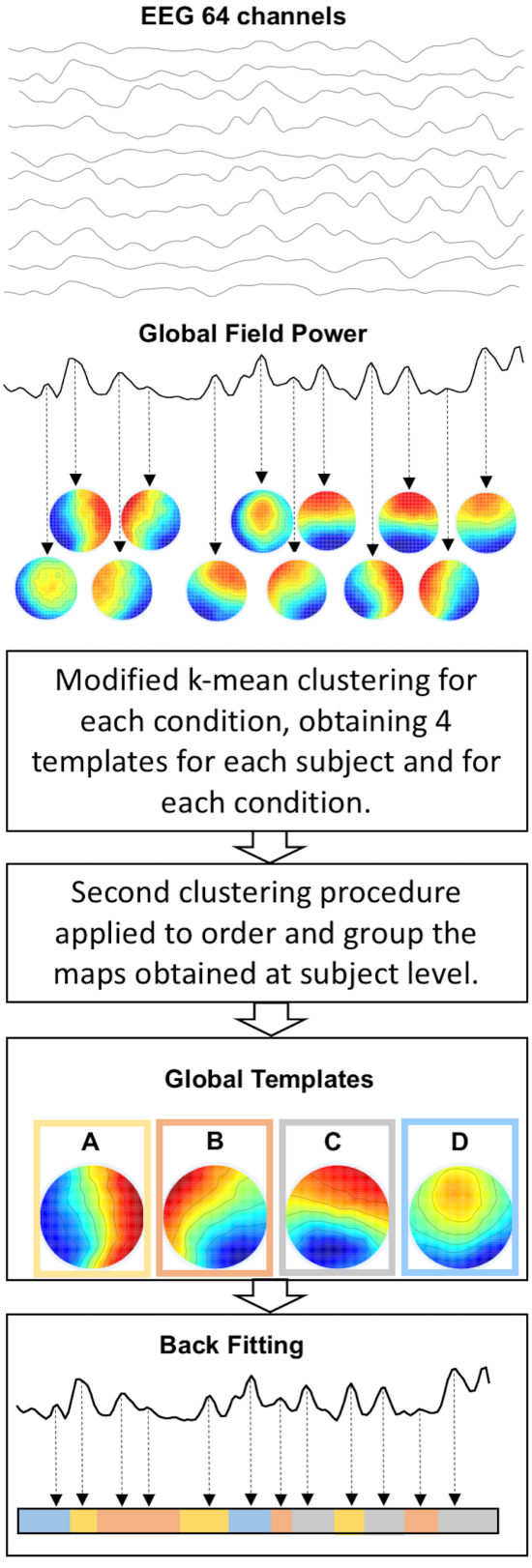

A. Topographic maps of the microstates

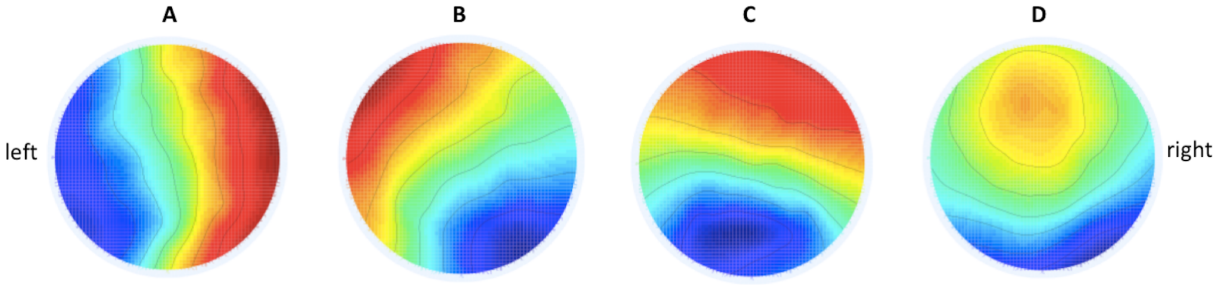

B. 95 % confidence intervals showing microstate coverage during the distinct Gf conditions

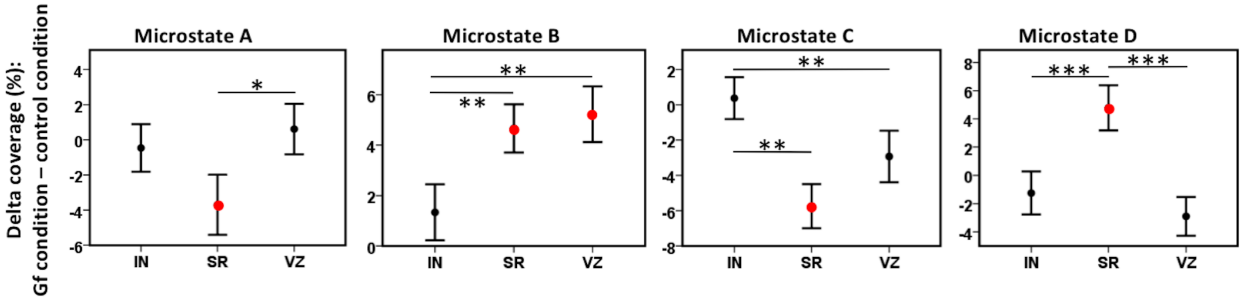

C. 95 % confidence intervals showing microstate duration during the distinct Gf conditions

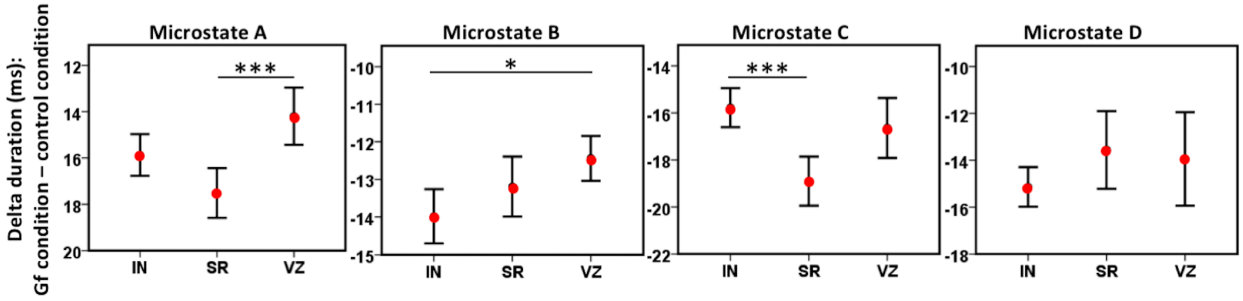

IN: Induction
SR: Spatial Relationships
VZ: Visualization

* $p < 0.05$ corrected ** $p < 0.005$ corrected *** $p < 0.001$ corrected

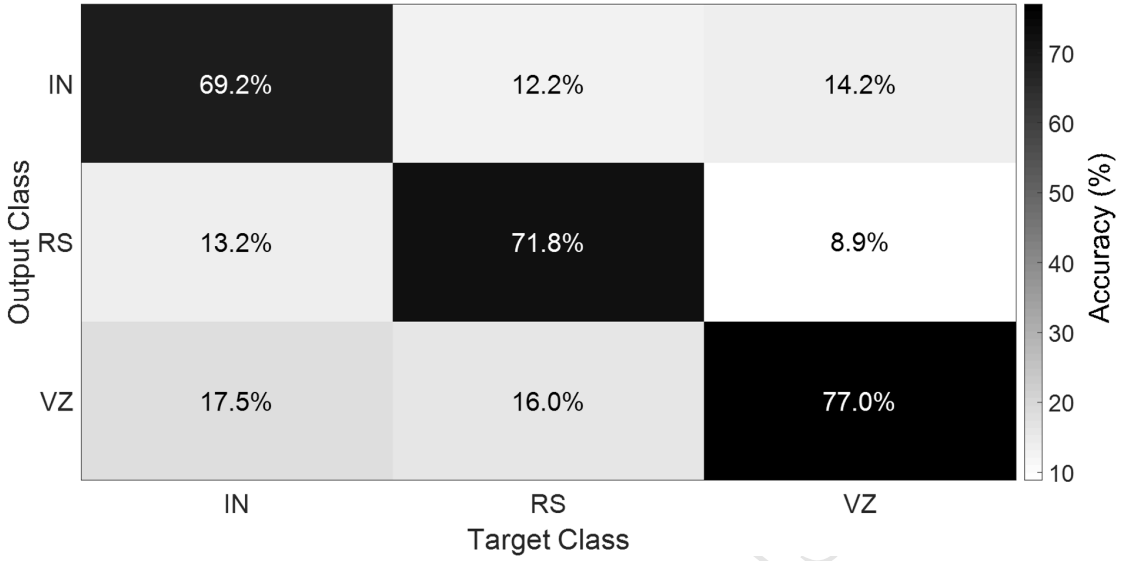

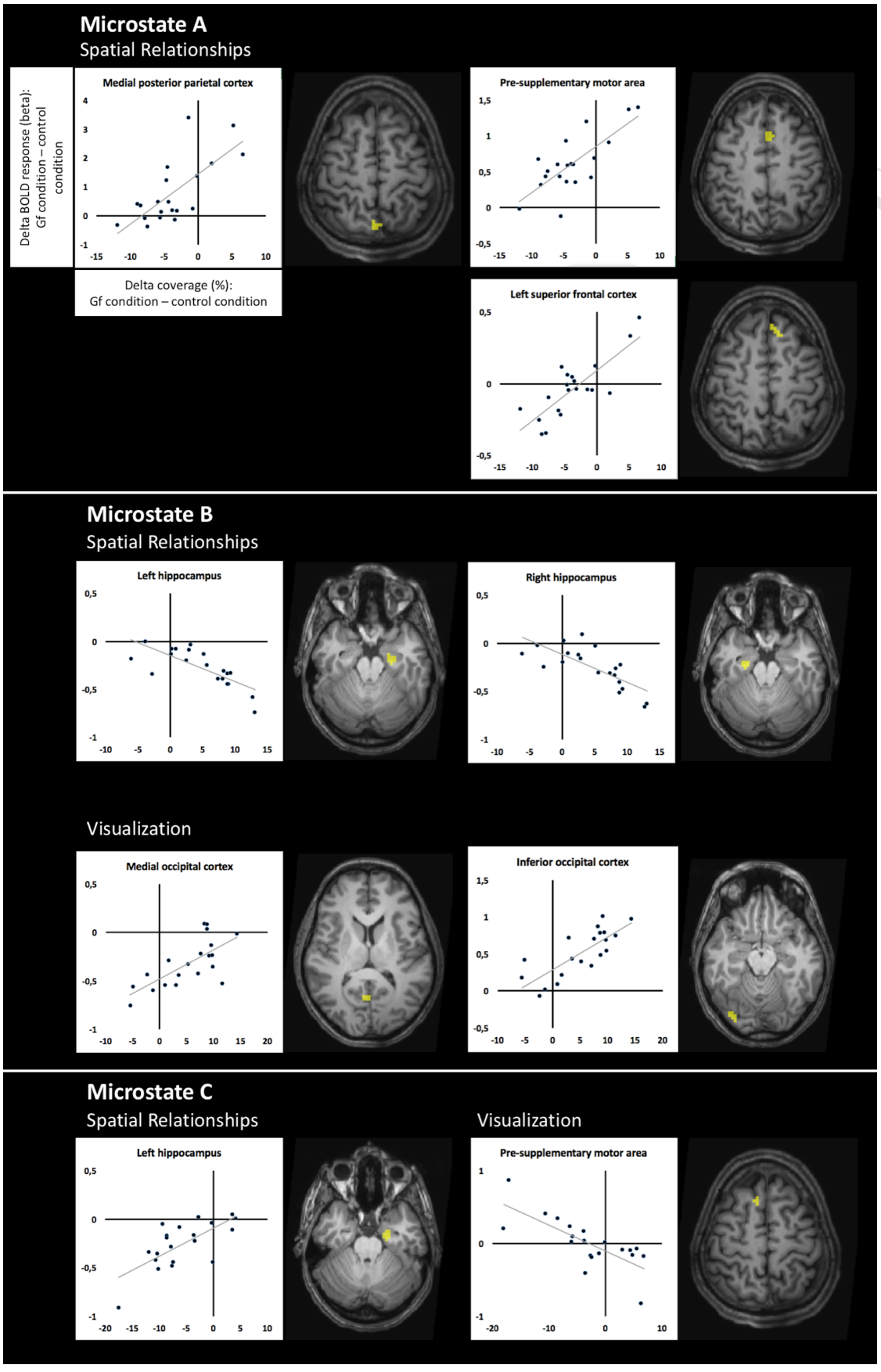
Microstate A
Spatial Relationships
Delta BOLD response (beta): Gf condition – control condition
Medial posterior parietal cortex
Pre-supplementary motor area
Left superior frontal cortex
Delta coverage (%): Gf condition – control condition
Microstate B
Spatial Relationships
Left hippocampus
Right hippocampus
Visualization
Medial occipital cortex
Inferior occipital cortex
Microstate C
Spatial Relationships
Left hippocampus
Visualization
Pre-supplementary motor area